Properties and predictive potential of the pre-ictal oscillatory dynamics in an *ex vivo* model of epileptiform activity in the different hippocampal subregions

Lida-Evmorfia Vagiaki[1,2], Dionysios Xydias[2,3], Maria Kefalogianni[2,4], Sotiris Psilodimitrakopoulos[2], Emmanuel Stratakis[2,4] and Kyriaki Sidiropoulou*[1,5]

1- Department of Biology, University of Crete

2- Institute of Electronic Structure and Laser, Foundation for Research and Technology Hellas

3-Department of Material Science and Technology, University of Crete

4-Department of Physics, University of Crete

5- Institute of Molecular Biology and Biotechnology, Foundation for Research and Technology Hellas

*corresponding author

Kyriaki Sidiropoulou

Associate Professor

Dept of Biology, University of Crete

IMBB-FORTH

e-mail: sidirop@imbb.forth.gr

Acknowledgements

This work was supported by the FLAG-ERA JTC 2017 project EPIGRAPH, funded nationally by GSRT (Greece, National Project Code: T18EPA2-00008) (ES) and the European Union's Horizon 2020 research and innovation program under the Marie Skłodowska-Curie grant agreement No 101007926 (KS).

Abstract

Neuronal oscillatory activity facilitates the transmission of information between neurons. However, abnormally synchronous neuronal activity results in the emergence of seizure-like activity (SLA). The hippocampus (HPC) is a brain area highly susceptible to SLA. The mechanisms leading to SLA are not yet well understood, although changes in neuronal oscillations have been suggested to exist in the time period before SLA onset. Anti-epileptic drugs, such as diazepam (DZP), a $GABA_A$ receptor agonist, and carbamazepine (CBZ), a sodium channel blocker, have significant anti-convulsant properties. However, their role in modulating the oscillatory activity within HPC subregions remains unclear. In our study, we used a high $[K^+]$ (HK^+) artificial cerebrospinal fluid (aCSF) solution to induce SLA in mouse HPC slices, which was detected using spontaneous local field potential (LFP) recordings. SLA activity was recorded in the three HPC subregions, namely CA1, CA3 and the dentate gyrus (DG). LFP analysis in the pre-ictal period revealed significant changes in the oscillatory activity compared to the absence of SLA and to ictal events. A classification algorithm revealed that the oscillatory dynamics, particularly in the CA1 subregion, can predict the emergence of an ictal event with high accuracy. Furthermore, we detected differential DZP and CBZ-induced changes in the oscillatory activity in the CA1, CA3 and DG. Imaging of neuronal activation in the *ex vivo* model of SLA, using the Fos protein as an activity marker, also revealed a subregion-dependent differential modulation following DZP and CBZ perfusion, which resembled the pattern of oscillatory activity changes. Therefore, the oscillatory dynamics could serve a potential electrophysiological biomarker for predicting seizure activity and are differentially modulated by anti-epileptic drugs.

Introduction

Epilepsy is a very common and serious neurological disorder, characterized by the occurrence of spontaneous recurrent seizure events (Liu, Tufa, et al., 2021). Seizure activity is a temporary manifestation of abnormally synchronized and excessive neuronal firing in the brain (Falco-Walter et al., 2018; Wu et al., 2021). The etiology of seizure events is diverse but associated with an imbalance of excitation-inhibition in neuronal networks (Ooi et al., 2023; van van Hugte et al., 2023).

Synchronous oscillatory activity is a form of correlated neuronal firing important for proper performance in cognitive tasks (Miller et al., 2018); however, hypersynchrony is observed in both in *in-vivo* mouse models of epilepsy and in epileptic patients (Gu et al., 2022; Mormann & Jefferys, 2013). In rodents, epileptic activity exhibits increased power in low- (delta and theta) and high-frequency (gamma) oscillations in the hippocampus (HPC) (Chou et al., 2020; Kitchigina, 2018; Lundstrom et al., 2021). These alterations in oscillatory activity have been observed in both the interictal (between seizures) and ictal (during seizures) periods, and are thought to contribute to the cognitive and behavioral deficits associated with epilepsy.

Identifying new targets for the identification and management of these epileptic events is imperative. Besides *in vivo* animal models, *ex vivo* models of epileptic activity in acute brain slices present a higher throughput and simplified approach to investigate the mechanisms of epileptogenesis and to evaluate novel therapeutic targets that reduce epileptic activity (Kreuzer et al., 2019). In particular, HPC brain slices represent a vital component of the neuronal networks involved in epilepsy, and are therefore commonly used in *ex vivo* studies on epilepsy (Avoli et al., 2002; Avoli & Jefferys, 2016; Dulla et al., 2018; Lazzarotto et al., 2021; Lisgaras & Scharfman, 2022; Panuccio et al., 2018; Raimondo et al., 2017). Earlier research has demonstrated that augmenting the concentration of extracellular potassium ions [K^+] in the perfusing solutions can elicit depolarization, increased firing rates and burst firing, as well (Grainger et al., 2018). These effects promote the development of both interictal and ictal-like activity patterns, establishing the high K^+ (HK^+) model as an *ex vivo* method for generating spontaneous recurrent seizure-like activity (SLA) (Du et al., 2016; Yaari et al., 1986)

Considerable research efforts currently aim at identifying electrophysiological biomarkers that can be used to predict the emergence of seizures (Elgohary et al., 2021; Hejazi & Motie Nasrabadi, 2019; Pinto et al., 2022; Traynelis et al., 2020; Yan et al., 2022; Yang et al., 2018). So far, seizure prediction models have focused on distinguishing between interictal and pre-ictal activity based on either the duration of each period or some time-frequency features of EEG signals, however the definition of the interictal phase remains unclear, and its duration can vary widely (Leal et al., 2023). Predictive models in models of epileptiform activity are rare (Abbas et al., 2019;

Graham et al., 2023) and render detailed study for predictive capabilities of various features difficult and fragmented.

Therefore, the objectives of this study are, on one hand, to determine whether oscillatory activity properties in the pre-ictal period can predict the onset of an ictal event, and, on the other hand, to explore alterations in oscillatory and cellular activity following perfusion of standard anti-epileptic drugs, such as diazepam (DZP) and carbamazepine (CBZ). The above two objectives were investigated in all three subregions of HPC, in an effort to identify possible differences among the three subregions, which participate in the HPC trisynaptic circuit.

Materials and Methods

Animals and Housing

Male and female C57Bl/6 mice, 30–60 days of age, were used for all experiments. Mice were group-housed (three to four per cage) and provided with food (standard mouse chow) and water *ad libitum*. The rooms vivarium was under a 12 h light/dark cycle (light on at 7:00 am) with controlled temperature (21 ±°C). All animal procedures comply with the ARRIVE guidelines and were performed according to the European and National ethical standards. All experiments were approved by the Department of Biology, University of Crete-Experimental Protocol Committee.

Brain Slice Preparation

Mice were euthanized under halothane anesthesia. The brain was quickly removed and placed in ice cold oxygenated artificial cerebrospinal fluid (aCSF) (95%O_2/5% CO_2) containing (in mM): 125 NaCl, 3.5 KCl, 26 $NaHCO_3$, 1 $MgCl_2$ and 10 glucose (pH =7.4, 310 mOsm/l). After the brain was blocked, the part containing the hippocampus was glued onto the stage of a vibratome (Leica, VT1000S, Leica Biosystems GmbH, Wetzlar, Germany). Brain slices (400μm) containing the HPC were placed in a submerged chamber containing oxygenated (95% O_2/5% CO_2) aCSF (in mM): 125 NaCl, 3.5 KCl, 26 $NaHCO_3$, 2$CaCl_2$, 1 $MgCl_2$ and 10 glucose (pH = 7.4, 315 mOsm/l) at 36,6 ºC. The brain slices were allowed to recover for at least 1 h in this chamber before recordings began.

Local Field Potential (LFP) Recordings and Data Analyses

The slices were placed in a temperature-controlled slice chamber at 32 ºC with 95% O_2-5% CO_2 under a stereoscope continuously perfused initially with normal aCSF containing (in mM): 125 NaCl, 3.5 KCl, 26 $NaHCO_3$, 2$CaCl_2$, 1 $MgCl_2$ and 10 glucose (pH = 7.4, 310 mOsm/l), followed by HK^+ aCSF (aCSF containing, in mM: 125 NaCl, 7.5 KCl, 26 $NaHCO_3$, 1 $MgCl_2$, 2 $CaCl_2$ and 10 glucose (pH = 7.4, 310 mOsm/l). To evaluate the effect of known anti-epileptic drugs, diazepam *(DZP)* (a GABA-A receptor agonist, C_{DZP}= 2μM) or carbamazepine *(CBZ)* (a sodium channel blocker, C_{CBZ}= 100μM) was diluted in HK^+ aCSF. Diazepam was acquired from the Pharmacy of the University General Hospital in Heraklion as a 5 mg/ml solution. CBZ was purchased from Sigma-Aldrich.

The recording electrode was filled with 3M NaCl and was positioned in CA1, CA3 or DG regions of distinct hippocampal brain slices. Spontaneous LFPs were amplified using the EXT-02F amplifier (National Instruments), digitized with ITC-18 (Instrutech, Inc.) and recorded in a computer running Windows10 with WinWCP software (Stratchclyde electrophysiology software). To measure the number of spikes the selectable high pass filter was adjusted at 3 Hz. When studying the oscillatory activity, the selectable high pass filter was adjusted at 0 Hz. The signal was low-pass filtered at 300Hz, in both types of recordings.

To analyze and measure the spontaneously occurring spiking events, referred to spikes from now on, the acquired 30 voltage traces of 32sec duration were first decimated by a factor of 10. The average and the standard deviation σb of the voltage signal were calculated. A spike was identified when any voltage response was detected at more than 5*σ of the average value.

To analyze the oscillatory activity, the time series of the voltage traces was transformed into frequency domains using a fast Fourier Transform (FFT) algorithm. The Power Spectral Density (PSD) was estimated for each frequency domain in logarithmic scale. The percentage of PSD from each frequency domain in relation to the PSD of the whole signal, defines a ratio referred as the rate of power (%). The rate of power (%) is estimated by the following equation:

$$Rate\ of\ Power(\%) = sum\left(\frac{Power\ of\ X\ oscillatory\ domain}{Total\ Power}\right) * 100$$

The ratio of the power spectrum was calculated for the following frequency domains: Delta (δ): 1–4 Hz, Theta (θ): 4–7 Hz, Alpha (α): 8–12 Hz, Beta (β): 13–30 Hz, Gamma (γ): 30–80 Hz and High Gamma (hγ): 80–200 Hz. All analysis was generated using custom-written procedures in MATLAB-R2023 (The MathWorks, Inc.).

Detection of seizure-like events (SLEs)

The beginning of an SLE was defined when the voltage signal was higher than 5σ above the average of the voltage signal (Pfammatter et al., 2018). An event ended when the signal decreased 4σ below the mean of the SLE. Seizure durations were manually measured as periods in which this rise crossed and remained above the threshold of 5σ for longer than 2sec. SLEs were considered to end if the signal returned to and stayed at baseline levels for longer than 2sec. We employed artifact rejection techniques to remove identified signals that were 15-fold larger in amplitude than the average spike amplitude (Sorokin et al., 2017).

Fos Immunochemistry Protocol

HPC brain slices (250μm), prepared as described above, were placed in a submerged chamber containing oxygenated normal aCSF and were allowed to equilibrate for 1 hr. Next, some of the brain slices were placed in a submerged chamber containing oxygenated HK^+ aCSF and some other brain slices were placed in a submerged chamber containing oxygenated HK^+ aCSF plus DZP (C_{DZP}= 2μM) or CBZ (C_{CBZ}= 100 μM) for 25 min. Following this incubation, all slices were transferred to different chambers containing oxygenated normal aCSF for another 1h. Finally, the slices were fixed in 4% paraformaldehyde solution (in different chambers) for 1h and, subsequently, washed with 0.1% PBS-Tween (PBS-T) and blocked overnight with 4% fetal bovine serum and 0.1% Triton in PBS-T. The next day, the slices were incubated with a primary antibody (c-Fos Antibody (E-8):sc-166940, Santa Cruz Biotechnology, Inc., 1:50 dilution) in 4% FBS and 0.1% Triton in PBS-T for 48 hours at 4°C. Afterwards, the slices were exposed to a secondary antibody (Goat Anti-Mouse IgG (H + L), CF®568, Biotium), were stirred for 5h at RT, mounted onto slides, and coverslipped with Mounting Medium with DAPI (ab104139) (Abcam plc.).

Imaging of Fos-stained slices

The slices were imaged in a custom-built laser raster-scanning, multiphoton microscope. By using a fs laser source, we excited two-photon fluorescence (2p-F) from c-Fos antibody.

Our custom-build multiphoton microscope (Suppl. Fig. 1) is using a 1030 nm fs laser (Flint, Light Conversion, Vilnius, Lithuania) as an excitation source, which is passing through a pair of galvanometric mirrors (6215 H, Cambridge Technology, Bedford, MA, USA) before entering into an inverted microscope (Axio Observer Z1, Carl Zeiss, Jena, Germany) (Kourgiantaki et al., 2020; Xydias et al., 2021). The beam is then reflected by a short pass dichroic mirror (FF700-SDi01, Semrock, Rochester, NY, USA) placed at the turret box of the microscope and is focused into the sample with a 20x 0.8NA objective-lens (Plan-Apochromat 20x/0.8NA, Carl Zeiss) or with a 40x 1.3NA objective-lens (Plan-Apochromat 40x/1.3NA, Carl Zeiss). The emitted fluorescence is collected by the same objective and is filtered by a short pass filter (FF01-680/SP, Semrock) to ensure that no laser light is reaching the detectors. Then a band-pass filter (FF1-562/40, Semrock) followed, which allowed passing the wavelengths in the range of 562 ± 20 nm, before reaching a detector, based on a photomultiplier tube PMT-blue (H9305-04, Hamamatsu, Hizuoka, Japan). The FF1-562/40 was used to detect the 2p-F from Fos antibody. Coordinate motion of the galvanometric mirrors and the detector for image acquisition was performed using custom-built Labview (National Instruments, Austin Texas, USA) software. The collage images were created by coordinate motion of the motorized sample stage of the microscope and image acquisition, using the Labview software.

Automated Counting of Activated Cells

All images were processed using the open-source ImageJ software, with the Fiji distribution (National Institute of Health and University of Wisconsin, USA) before used for cell counting. CellProfiler 4.2.5 (http://www.cellprofiler.org/index.shtmL) was used for automated counting the Fos expressing cells. All images were of the same total area covered by cells of 1200μm^2 for each subfield. The CellProfiler software was first used to measure the range of a typical diameter of cells 15-140, in pixel units. The Threshold method used was Minimum Cross-Entropy with lower and upper bounds 0.15-1.0, smoothing scale 1.3488 and correction factor 1.0 (Suppl. Fig.2).

Statistical Analysis

One-way ANOVA analysis was performed for spiking and oscillatory activity analysis, followed by the post hoc Tukey test for within group analysis. Statistical analysis was performed with GraphPad Prism.

Results

Effects of an *ex vivo* model of SLA on the number of spikes in HPC brain slices

We first evaluated the effects of HK^+ *ex vivo* model of SLA on the spontaneous activity. We recorded the number of elicited spikes in the CA1, CA3 and DG subfields following HK^+ perfusion in HPC brain slices of adult male and female mice. Perfusion of HK^+ aCSF significantly increases the number of spikes (Fig. 1A) and induces SLA in all three HPC subregions, as evidenced by the representative traces (Fig. 1B).

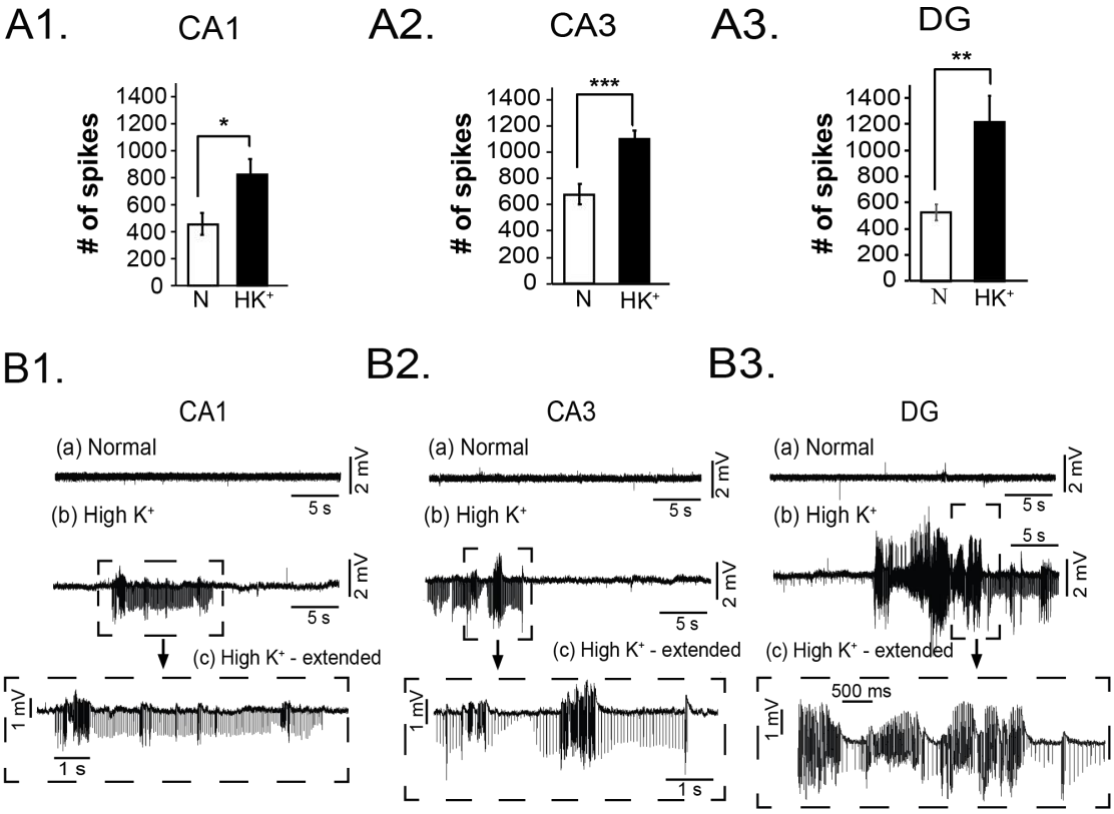

Figure 1. Effect of HK^+ aCSF on the spiking activity of CA1, CA3 and DG subfields

(A1) A significant increase in the number of spontaneous events after HK^+ perfusion in the CA1 (t-test, p=0,02).*

*(A2) Graph showing that the number of spontaneous events is significantly increased following perfusion of HK^+ in the CA3 subfield (t-test, p***=0,0007).*

*(A3) Graph indicates a significant increase after the perfusion of HK^+ aCSF compared to the N aCSF (t-test, p**=0,009) in the DG.*

(C1-3) Representative voltage traces following N and HK+ perfusion. (C1.c-C3.c) Dotted lines indicate extended voltage traces showing ictal discharges.

Pre-ictal analysis of the oscillatory activity across the HPC subfields

We next aimed to determine whether the oscillatory dynamics differ between the pre-ictal period during the perfusion of the HK^+ aCSF and the period before perfusion of HK^+ aCSF when no SLA is present (non-ictal) in the same HPC slice. Our results revealed no difference in the detected spontaneous events between the pre-ictal period and the period before perfusion of HK^+ aCSF. We first identified ictal discharges and analyzed the oscillatory patterns of 1sec segments at different time points relative to the start of ictal discharges. Specifically, we analyzed the 10th, 5th and 1st second prior to the start of the ictal discharge (pre-ictal), as well as various 1sec segments within a 10sec recording duration under the normal aCSF condition (non-ictal) in the same brain slice (Fig. 2). Our temporal analyses were conducted in recordings from all three HPC subfields. The results from the analyses between the non-ictal and pre-ictal segments revealed significant increases in the rate of power observed between all 1sec pre-ictal segments and the non-ictal segment. Specifically, the increased rate of power between the non-ictal and pre-ictal segments were found in θ, α, β and hγ frequency domains in all subfields. However, the differences in oscillatory dynamics were more substantial within the CA1 and CA3 subfields, compared to the DG (Fig. 2).

Moreover, we compared the 1st second of the ictal period to the 1sec segments of the pre-ictal period. As expected, there were large and significant differences in the rate of power of all frequency domains between the 10th, 5th or 1st second in the pre-ictal period and the 1st second of the ictal period in CA1 (Suppl. Fig.3), CA3 (Suppl. Fig.4). and DG subfields (Suppl. Fig.5).

Consequently, these results suggest that the oscillatory dynamics during the 10sec pre-ictal period are significantly different from the oscillatory dynamics during the non-ictal period, but also from the period of ictal discharges.

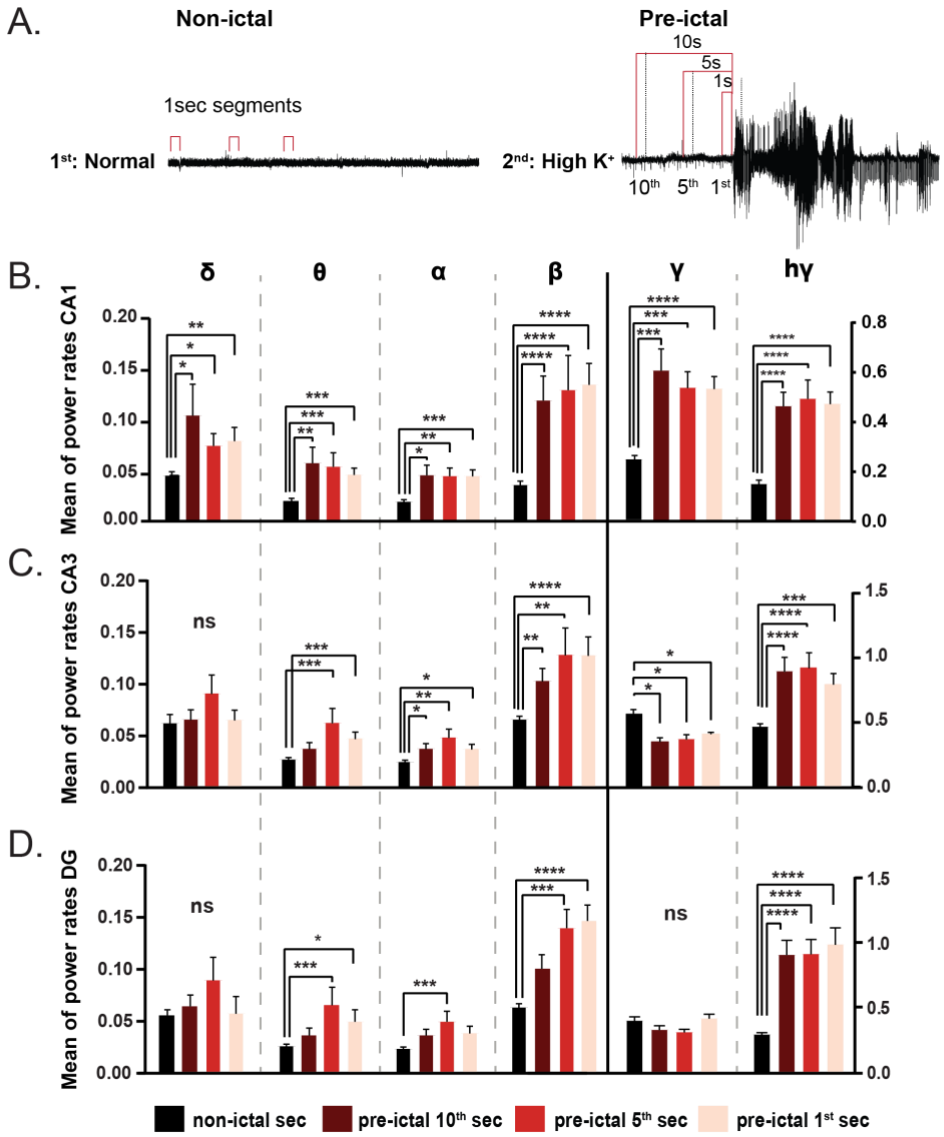

Figure 2: Inter-temporal comparative analysis of the rate of power of oscillatory events across all oscillatory bands between a non-ictal-segment and the pre-ictal 1-second segments in HPC.

(A) Voltage traces from LFP recordings during perfusion of normal (left) or HK$^+$ aCSF (right). Representation of the designated time periods defined in both normal (various segments) and HK$^+$ aCSF (three 1-second segments) recordings.

*(B-D) Graph showing the rate of power in the low, mid and high frequencies of oscillatory events during distinct 1-sec intervals in the CA1 (B), CA3 (C) and DG (D) subfields under normal and HK$^+$ aCSF perfusion. A significant difference in the rate of power between the pre-ictal and non-ictal 1-sec segments in the CA1 (One-way ANOVA F(23, 594)=49,50, p***<0,0001) (B.), CA3 (One-way ANOVA F(23, 558)=72,97,*

*p****<0,0001) (C.), and DG (One-way ANOVA F(23,498)=70,22, p****<0,0001) (D.) subfields. [for within groups statistical analysis, see Suppl. Table1-3].*

Prediction of the SLEs based on the oscillatory activity during the 10sec pre-ictal period

Based on the observed differences between the pre-ictal and non-ictal periods, as well as between the pre-ictal period and the ictal period, we tested whether the oscillatory dynamics in the pre-ictal period can predict the emergence of an ictal event. To achieve this, the power rate of the different frequency domains during the 10th and 5th seconds before the emergence of an ictal event, as well as in 1-sec segments when brain slices were perfused with normal aCSF (i.e. in the absence of ictal events, non-ictal) were used to train and test a classification algorithm using Linear Discriminant Analysis (LDA). Initially, different models were trained using values from all 6 frequency domains during the 10th second of the pre-ictal period across the 3 HPC subregions. The results indicated that SLEs in CA1 region can be predicted with a much better accuracy, compared to SLEs in the CA3 and DG regions (Fig. 3A). The sensitivity and specificity of the model were also notably better (100%) for the CA1 SLEs compared to that of the CA3 and DG regions (Fig. 3C and D).

Shuffling of the data that were used to train and test the CA1 LDA model resulted in significantly poorer performance (70% train accuracy, 64% test accuracy, 33.3% sensitivity and 72% specificity). Furthermore, we tested whether oscillatory dynamics during the 5th second could predict the emergence of SLEs in the CA1 region and found that, similar to the 10th second, an LDA algorithm could reliably predict the emergence of SLEs (90% train accuracy, 92% test accuracy, 100% sensitivity, 92% specificity). Finally, we wanted to determine whether different frequencies could more accuretely predict the emergence of an SLE. We trained and tested different LDA models using values from specific frequency domains. High-frequency values (γ and hγ) provided the most accurate predictions of SLE emergence (with 90% accuracy and above), while lower-frequency domains still showed predictive ability , albeit with lower accuracy (between 80 and 90%).

Therefore, our results suggest that an LDA algorithm trained on oscillatory dynamics can predict the emergence of ictal events 5 to10 seconds before their onset.

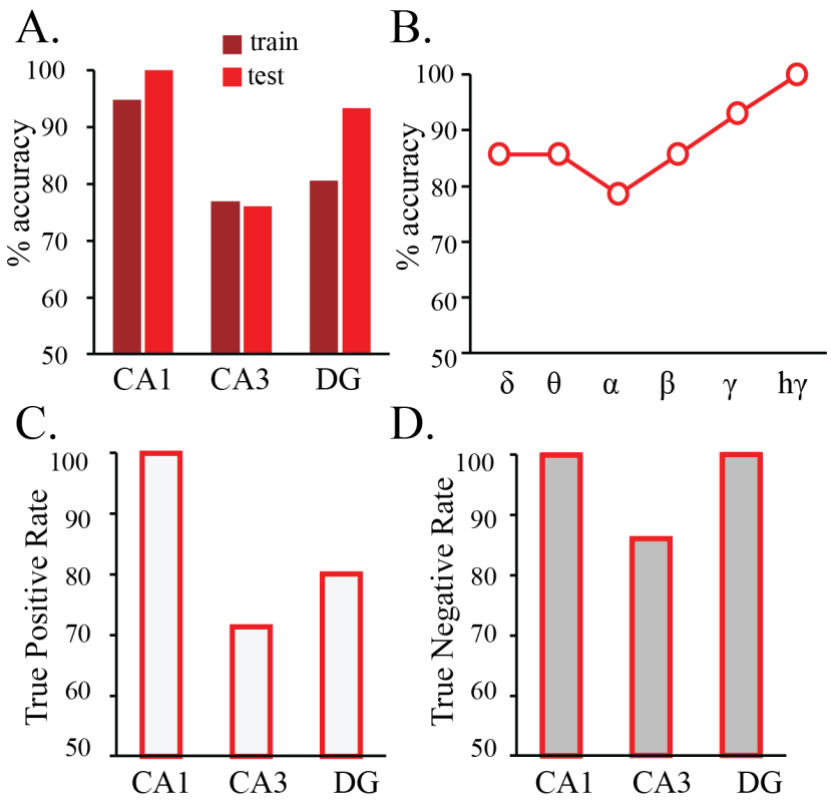

Figure 3: Prediction of SLEs based on the oscillatory dynamics during the 10th second of the pre-ictal period using LDA.

(A) Total accuracy following training and testing of Linear Discriminant models using the values for all frequency domains for the CA1, CA3 and DG subregions.

(B) Total accuracy following testing of the trained models for different frequencies of the CA1 region, separately.

(C) Sensitivity of test set of the linear discriminant models from the different subregions.

(D) Specificity of test set of the linear discriminant models from the different subregions

Effects of DZP and CBZ administration on the Oscillatory Activity in HPC brain slices

Given the importance of oscillatory dynamics in predicting SLA, we wanted to investigate the modulation of oscillatory activity in the three HPC subregions following perfusion of DZP or CBZ, two well-known anti-epileptic drugs (Fig. 4). In the CA1 subfield, DZP or CBZ did not result in significant changes in the rate of power of the oscillatory events at all frequency domains. In the CA3 subfield, perfusion of the anti-

epileptic drugs, DZP or CBZ significantly decreased the rate of power in the hγ frequency domain. In the DG subfield, there was a significant effect of treatment on the rate of power in γ and hγ frequencies. Moreover, perfusion of DZP-aCSF resulted in a trend of decrease in the power rates of β oscillations.

Thus far, our results indicate subregion-specific adaptations in the oscillatory activity, following perfusion of HK^+, DZP and CBZ in HPC brain slices.

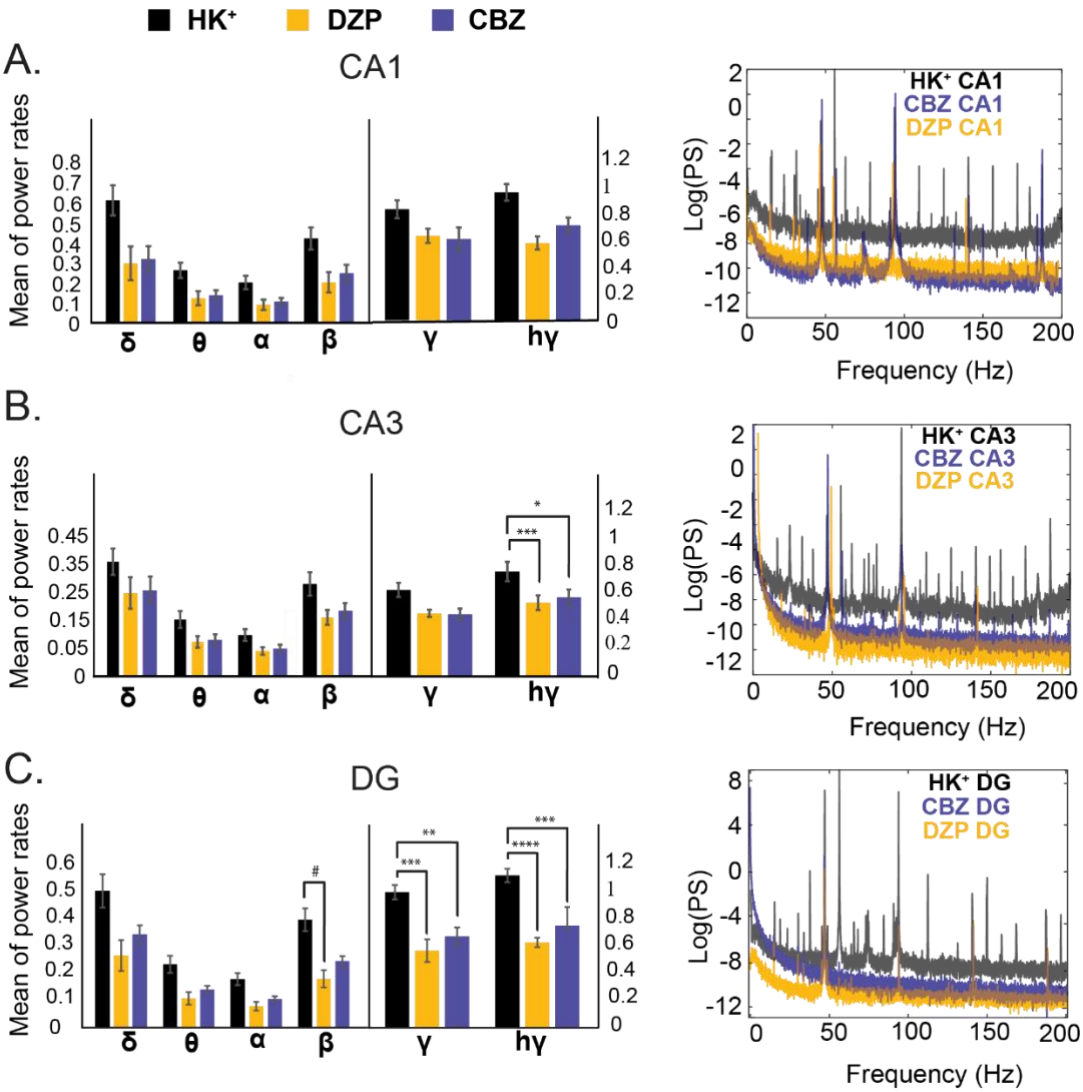

Figure 4: Adaptations in the oscillatory activities between different aCSF conditions within the CA1, CA3 and DG subfields.

(A-C), (left) Graphs showing the rate of power in the 3 conditions, HK^+, HK^+ plus DZP and HK^+ aCSF plus CBZ in the CA1 (A), CA3 (B) and DG (C) regions. (right) PSD representative traces illustrating the peaks of power of the synchronous oscillatory activity recorded in the HPC following treatment with DZP or CBZ. [For CA1, one-

*way ANOVA F(17,336)=13,44, p^{****}<0,0001, post-hoc Tukey test, within groups (HK^+ vs DZP or CBZ) p>0,05 (n=43 slices from 25 mice for the perfusion of HK^+ aCSF, n=9 slices from 5 mice for the perfusion of 2 µM DZP or 100 µM CBZ)]. [For CA3, one-way ANOVA F(17,234)=34,03, p****<0,0001, post-hoc Tukey test, (HK^+ vs DZP) p^{***}<0,0005, (HK^+ vs CBZ) p^{*}=0,03 for hγ (n=18 slices from 16 mice for the perfusion of HK^+ aCSF, n=8 slices from 8 mice for the DZP-aCSF, n=10 slices from 8 mice for the CBZ-aCSF)]. [For DG, one-way ANOVA F(17,144)=33,95, p****<0,0001, post-hoc Tukey test, (HK^+ vs DZP) p****<0,0001 for γ and hγ, (HK^+ vs CBZ) p**=0,004 for γ and p***=0,0005 for hγ (n=16 slices from 14 mice for the perfusion of HK^+ aCSF, n=6 slices from 6 mice for DZP-aCSF, n=8 slices from 6 mice)].*

Effects of DZP or CBZ administration on the number of Fos expressing cells in the hippocampus using multiphoton imaging

Since the electrophysiological recordings in the different subregions were not performed concurrently, we utilized an imaging approach to further investigate differences between the CA1, CA3 and the DG subregions. We performed Fos immunofluorescence in HPC brain slices after the administration of the same perfusing conditions used in the electrophysiological recordings. Perfusion of DZP in the presence of HK^+ aCSF resulted in significant reduction of the number of Fos positive cells in the CA1, CA3 and DG subfields. Perfusion of CBZ also significantly reduced the number of Fos positive cells in the CA3 and DG subfields, but not in the CA1 region (Fig. 5).

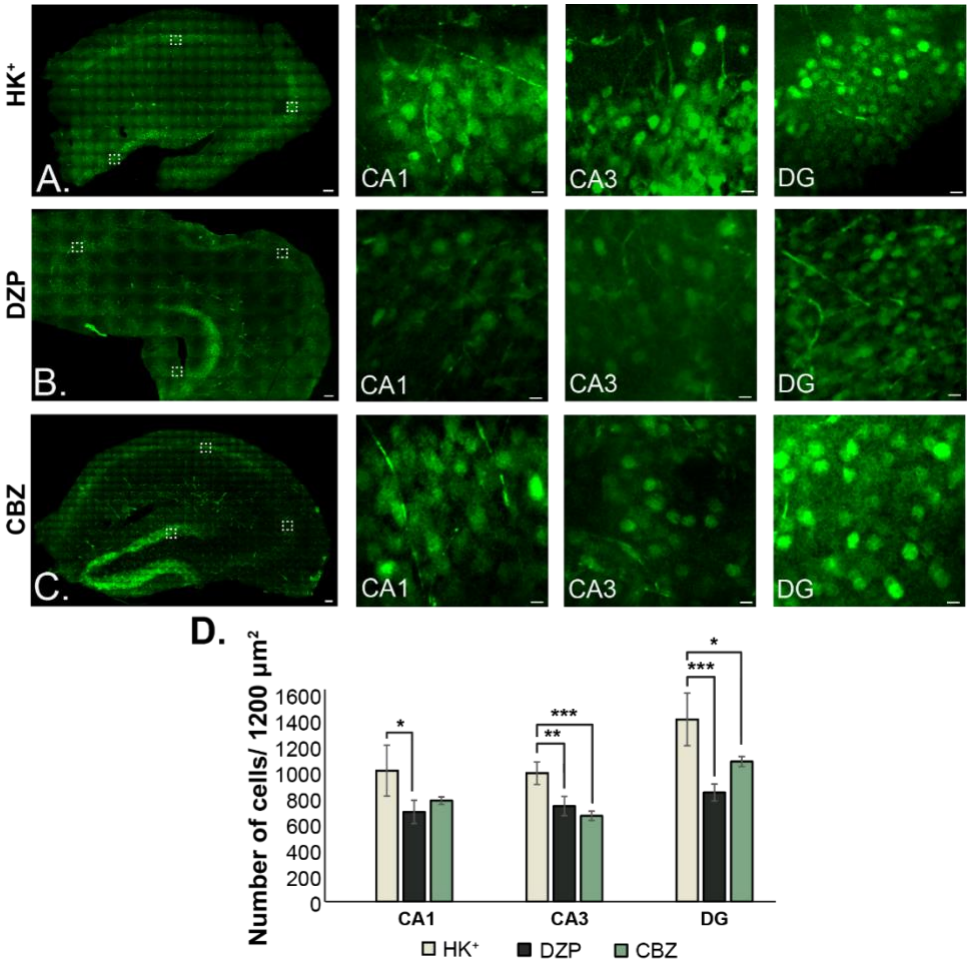

Figure 5: Expression of c- Fos in the HPC. (A-C) Representative multiphoton images after the perfusion of (A) HK^+, (B) DZP and (C) CBZ aCSF, scale bar 100µm for HPC from one hemisphere and 10µm for CA1, CA3 and DG separately. Dotted squares display representative images for the 3 subfields. (D) Number of activated cells that were identified after the different perfusing conditions in the 3 subfields. (CA1: one way ANOVA (F(2,28)=5,53, p**=0,004; post-hoc Tukey test DZP<HK^+ p*=0,02, CBZ<HK+ p=0,14; CA3: one way ANOVA (F(2,27)=6,73, p***=0,001; post-hoc Tukey test DZP<HK^+ p**=0,01, CBZ<HK^+ p***=0,001; DG: one way ANOVA (F(2,26)=7,77, p***=0,0002; ; post-hoc Tukey test DZP<HK^+ p***=0,001, CBZ<HK^+ p*=0,04).

Discussion

Our study revealed a significant, subregion-specific role of neuronal oscillations in both predicting the emergence of SLA and its modulation by anti-epileptic drugs. Firstly,

our results showed that the oscillatory dynamics in the 10-sec pre-ictal period are significantly different compared to the oscillatory dynamics in the non-ictal period and the onset of the ictal period. Additionally, the oscillatory dynamics during the 10th and 5th seconds could predict the emergence of SLA with high accuracy, especially in the CA1 region. Secondly, anti-epileptic drugs (DZP and CBZ) modulated high-frequency neuronal oscillations, primarily in the DG.

Prediction of SLEs

In this study, we highlight the significant differences in oscillatory dynamics across the pre-ictal, non-ictal and ictal periods. Specifically, power rates of different oscillatory frequencies in the pre-ictal period are significantly higher compared to non-ictal activity but lower compared to ictal activity. Therefore, based on these differences, we investigated whether these power rates could predict the emergence of SLEs and found that prediction is possible with high accuracy, specificity and sensitivity, particularly in the CA1 region.

Most predictive models have utilized clinical datasets obtained from either intracranial EEG or scalp EEG and aim to distinguish between the interictal and pre-ictal periods (Hejazi & Motie Nasrabadi, 2019) or between the early and late pre-ictal states reached ~80% of accuracy (Elgohary et al., 2021). Yan et al., designed a seizure predictive model and used EEG recordings from patients to predict the occurrence of a seizure outbreak. The seizure prediction horizon was set at 3 min and the accuracy of the prediction was about ~90% (Yan et al., 2022). Yang et al., trained an SVM algorithm with permutation entropy datasets from EEG recordings and obtained an average sensitivity ~90% (Yang et al., 2018). Sheybani et al., used multisite intracortical recordings from patients and detected increased δ and θ activity during the interictal period (Sheybani et al., 2021).

There are only a couple of animal or ex vivo studies applying predictive algorithms for epileptic discharge detection. The studies have used various statistical metrices of spiking activity (Abbas et al., 2019) or ion concentration changes (Graham et al., 2023) to predict the emergence of an epileptic event.

In our study, the power rates of neuronal oscillations at different frequencies measuredduring the 10th and 5th seconds before an ictal event in the CA1 were able to predict the imminent occurrence of an ictal event with 100% test accuracy. Isolated

frequency ranges, particularly high frequencies (γ and hγ) also predicted SLA with over 90% accuracy. Conversely, prediction accuracy based on the oscillatory dynamics in the CA3 and DG subregions was below 90%. Consequently, our results suggests that the oscillatory dynamics could predict the emergence of an ictal event in a region-specific manner. Further experiments investigating various predictive features could provide valuable insights for developing further patient-specific analyses.

Differential modulation of oscillatory dynamics across the 3 HPC subregions during DZP or CBZ administration

Perfusion of the HK^+ aCSF elicited tonic SLEs in all three HPC subfields, aligned with previous reports (Jensen & Durand, 2007; Traynelis & Dingledine, 1988). Both slow and fast neuronal oscillation are significantly enhanced during SLA, compared to the pre-ictal and non-ictal activity. These results align with previous reports that observed that the peak rates of the mid and high frequency domains exhibit higher levels during the ictal discharges (Benedek et al., 2016; Pinheiro et al., 2020; Sorokin et al., 2016).

Additionally, the power rates of different frequency domains during oscillatory activity were differentially modulated in the different HPC subfields following administration of DZP and CBZ. Our results further suggest that the oscillatory dynamics of the CA3 and DG subfields are more susceptible to modulation by DZP or CBZ compared to the CA1 region. These results are consistent with a previous study conducted in mice with EEG recordings, in which DZP administration resulted in a reduction in the synchronicity of the oscillatory activity (McKillop et al., 2021).

Furthermore, the sensitivity to SLE inhibition was different among the three subfields (CA1, CA3, DG) after DZP and CBZ perfusion. In particular, the CA regions are more sensitive to DZP and CBZ with regards to the number of spikes, compared to the DG subfield. Interictal spikes in the DG subfield have also been found to be less sensitive to the administration of the CBZ aCSF in previous studies (D'Antuono et al., 2010; Duveau et al., 2016; Liu, Zhang, et al., 2021). Regarding the effectiveness of DZP in the three different subfields, one key factor could be the distribution of $GABA_A$ receptor subtypes within the CA1, CA3 and DG regions. Different $GABA_A$ receptor subtypes have distinct pharmacological properties and regional distributions. A previous study has shown that the DG expresses a higher proportion of $GABA_A$ receptors containing the α5 subunit, which have been implicated in cognitive functions such as learning and

memory. According to a previous study conducted in cell cultures from HPC neurons, activation of these receptors by benzodiazepines may have different effects compared to receptors in other brain regions, resulting in reduced effectiveness (Caraiscos et al., 2004). Similarly, CBZ has also been shown to be ineffective in reducing interictal spiking in EEG recordings in an intrahippocampal kainate mouse model or in field potentials from mouse HPC brain slices after the perfusion of a high-bicarbonate aCSF (Duveau et al., 2016; Liu, Tufa, et al., 2021).

Expression of Fos protein and oscillatory dynamics

In our study, the expression of c-Fos was significantly decreased in the CA3 and DG subfields following the perfusion of DZP or CBZ, but not in CA1. Consequently, our results suggest that Fos activation could be modulated by DZP and CBZ in an HPC subregion-dependent manner. The adaptation pattern observed with Fos modulation (more in CA3 and DG and less in CA1) resembled the pattern observed in oscillatory dynamics modulation in the three HPC subregions. Correlated changes of Fos expression and oscillatory dynamics have been identified in other reports as well (Vila-Merkle et al., 2023; Wang et al., 2021). Taken together, the expression of c-Fos could possibly serve as a molecular biomarker for the network synchronicity.

References

Abbas, M. K., Raza, M. L., Zaidi, S. S. H., Khan, B. M., & Heinemann, U. (2019). Seizure forecasting using single robust linear feature as correlation vector of seizure-like events in brain slices preparation in vitro. Neurological Research, 41(2), 99–109. https://doi.org/10.1080/01616412.2018.1532481

Avoli, M., D'Antuono, M., Louvel, J., Köhling, R., Biagini, G., Pumain, R., D'Arcangelo, G., & Tancredi, V. (2002). Network and pharmacological mechanisms leading to epileptiform synchronization in the limbic system in vitro. Progress in Neurobiology, 68(3), 167–207. https://doi.org/10.1016/S0301-0082(02)00077-1

Avoli, M., & Jefferys, J. G. R. (2016). Models of drug-induced epileptiform synchronization in vitro. Journal of Neuroscience Methods, 260, 26–32. https://doi.org/10.1016/j.jneumeth.2015.10.006

Benedek, K., Berényi, A., Gombkötő, P., Piilgaard, H., & Lauritzen, M. (2016). Neocortical gamma oscillations in idiopathic generalized epilepsy. Epilepsia, 57(5), 796–804. https://doi.org/10.1111/epi.13355

Caraiscos, V. B., Elliott, E. M., You-Ten, K. E., Cheng, V. Y., Belelli, D., Newell, J. G., Jackson, M. F., Lambert, J. J., Rosahl, T. W., Wafford, K. A., MacDonald, J. F., & Orser, B. A. (2004). Tonic inhibition in mouse hippocampal CA1 pyramidal neurons is mediated by α5 subunit-containing γ-aminobutyric acid type A receptors. Proceedings of the National Academy of Sciences, 101(10), 3662–3667. https://doi.org/10.1073/pnas.0307231101

Chou, P., Wang, G.-H., Hsueh, S.-W., Yang, Y.-C., & Kuo, C.-C. (2020). Delta-Frequency Augmentation and Synchronization in Seizure Discharges and Telencephalic Transmission. IScience, 23(11), 101666. https://doi.org/10.1016/j.isci.2020.101666

D'Antuono, M., Köhling, R., Ricalzone, S., Gotman, J., Biagini, G., & Avoli, M. (2010). Antiepileptic drugs abolish ictal but not interictal epileptiform discharges in vitro. Epilepsia, 51(3), 423–431. https://doi.org/10.1111/j.1528-1167.2009.02273.x

Du, M., Li, J., Wang, R., & Wu, Y. (2016). The influence of potassium concentration on epileptic seizures in a coupled neuronal model in the hippocampus. Cognitive Neurodynamics, 10(5), 405–414. https://doi.org/10.1007/s11571-016-9390-4

Dulla, C. G., Janigro, D., Jiruska, P., Raimondo, J. V., Ikeda, A., Lin, C. K., Goodkin, H. P., Galanopoulou, A. S., Bernard, C., & Curtis, M. (2018). How do we use in vitro models to understand epileptiform and ictal activity? A report of the <scp>TASK</scp> 1- <scp>WG</scp> 4 group of the <scp>ILAE</scp> / <scp>AES</scp> Joint Translational Task Force. Epilepsia Open, 3(4), 460–473. https://doi.org/10.1002/epi4.12277

Duveau, V., Pouyatos, B., Bressand, K., Bouyssières, C., Chabrol, T., Roche, Y., Depaulis, A., & Roucard, C. (2016). Differential Effects of Antiepileptic Drugs on Focal Seizures in the Intrahippocampal Kainate Mouse Model of Mesial Temporal Lobe Epilepsy. CNS Neuroscience & Therapeutics, 22(6), 497–506. https://doi.org/10.1111/cns.12523

Elgohary, S., Khalil, M. I., & Eldawlatly, S. (2021). A two-stage classification framework for epileptic seizure prediction using EEG wavelet-based features. In Big Data in Psychiatry #x0026; Neurology (pp. 263–286). Elsevier. https://doi.org/10.1016/B978-0-12-822884-5.00021-0

Falco-Walter, J. J., Scheffer, I. E., & Fisher, R. S. (2018). The new definition and classification of seizures and epilepsy. Epilepsy Research, 139, 73–79. https://doi.org/10.1016/j.eplepsyres.2017.11.015

Graham, R. T., Parrish, R. R., Alberio, L., Johnson, E. L., Owens, L., & Trevelyan, A. J. (2023). Optogenetic stimulation reveals a latent tipping point in cortical networks during ictogenesis. Brain, 146(7), 2814–2827. https://doi.org/10.1093/brain/awac487

Grainger, A. I., King, M. C., Nagel, D. A., Parri, H. R., Coleman, M. D., & Hill, E. J. (2018). In vitro Models for Seizure-Liability Testing Using Induced Pluripotent Stem Cells. Frontiers in Neuroscience, 12. https://doi.org/10.3389/fnins.2018.00590

Gu, B., Levine, N. G., Xu, W., Lynch, R. M., Pardo-Manuel de Villena, F., & Philpot, B. D. (2022). Ictal neural oscillatory alterations precede sudden unexpected death in epilepsy. Brain Communications, 4(2). https://doi.org/10.1093/braincomms/fcac073

Hejazi, M., & Motie Nasrabadi, A. (2019). Prediction of epilepsy seizure from multi-channel electroencephalogram by effective connectivity analysis using Granger causality and directed transfer function methods. Cognitive Neurodynamics, 13(5), 461–473. https://doi.org/10.1007/s11571-019-09534-z

Jensen, A. L., & Durand, D. M. (2007). Suppression of axonal conduction by sinusoidal stimulation in rat hippocampus in vitro. Journal of Neural Engineering, 4(2), 1–16. https://doi.org/10.1088/1741-2560/4/2/001

Kitchigina, V. F. (2018). Alterations of Coherent Theta and Gamma Network Oscillations as an Early Biomarker of Temporal Lobe Epilepsy and Alzheimer's Disease. Frontiers in Integrative Neuroscience, 12. https://doi.org/10.3389/fnint.2018.00036

Kourgiantaki, A., Tzeranis, D. S., Karali, K., Georgelou, K., Bampoula, E., Psilodimitrakopoulos, S., Yannas, I. V., Stratakis, E., Sidiropoulou, K., Charalampopoulos, I., & Gravanis, A. (2020). Neural stem cell delivery via porous collagen scaffolds promotes neuronal differentiation and locomotion recovery in spinal cord injury. Npj Regenerative Medicine, 5(1), 12. https://doi.org/10.1038/s41536-020-0097-0

Kreuzer, M., García, P. S., Brucklacher-Waldert, V., Claassen, R., Schneider, G., Antkowiak, B., & Drexler, B. (2019). Diazepam and ethanol differently modulate neuronal activity in organotypic cortical cultures. BMC Neuroscience, 20(1), 58. https://doi.org/10.1186/s12868-019-0540-6

Lazzarotto, G., Klippel Zanona, Q., Cagliari Zenki, K., & Calcagnotto, M. E. (2021). Effect of Memantine on Pentylenetetrazol-induced Seizures and EEG Profile in Animal Model of Cortical Malformation. Neuroscience, 457, 114–124. https://doi.org/10.1016/j.neuroscience.2020.12.039

Leal, A., Curty, J., Lopes, F., Pinto, M. F., Oliveira, A., Sales, F., Bianchi, A. M., Ruano, M. G., Dourado, A., Henriques, J., & Teixeira, C. A. (2023). Unsupervised EEG preictal interval identification in patients with drug-resistant epilepsy. Scientific Reports, 13(1), 784. https://doi.org/10.1038/s41598-022-23902-6

Lisgaras, C. P., & Scharfman, H. E. (2022). Robust chronic convulsive seizures, high frequency oscillations, and human seizure onset patterns in an intrahippocampal kainic acid model in mice. Neurobiology of Disease, 166, 105637. https://doi.org/10.1016/j.nbd.2022.105637

Liu, H., Tufa, U., Zahra, A., Chow, J., Sivanenthiran, N., Cheng, C., Liu, Y., Cheung, P., Lim, S., Jin, Y., Mao, M., Sun, Y., Wu, C., Wennberg, R., Bardakjian, B., Carlen, P. L., Eubanks, J. H., Song, H., & Zhang, L. (2021). Electrographic Features of Spontaneous Recurrent Seizures in a Mouse Model of Extended Hippocampal Kindling. Cerebral Cortex Communications, 2(1). https://doi.org/10.1093/texcom/tgab004

Liu, H., Zhang, S., & Zhang, L. (2021). Epileptiform activity in mouse hippocampal slices induced by moderate changes in extracellular Mg2+, Ca2+, and K+. BMC Neuroscience, 22(1), 46. https://doi.org/10.1186/s12868-021-00650-3

Lundstrom, B. N., Brinkmann, B. H., & Worrell, G. A. (2021). Low frequency novel interictal EEG biomarker for localizing seizures and predicting outcomes. Brain Communications, 3(4). https://doi.org/10.1093/braincomms/fcab231

McKillop, L. E., Fisher, S. P., Milinski, L., Krone, L. B., & Vyazovskiy, V. V. (2021). Diazepam effects on local cortical neural activity during sleep in mice. Biochemical Pharmacology, 191, 114515. https://doi.org/10.1016/j.bcp.2021.114515

Miller, E. K., Lundqvist, M., & Bastos, A. M. (2018). Working Memory 2.0. Neuron, 100(2), 463–475. https://doi.org/10.1016/j.neuron.2018.09.023

Mormann, F., & Jefferys, J. G. R. (2013). Neuronal Firing in Human Epileptic Cortex: The Ins and Outs of Synchrony during Seizures. Epilepsy Currents, 13(2), 100–102. https://doi.org/10.5698/1535-7597-13.2.100

Ooi, Q. Y., Qin, X., Yuan, Y., Zhang, X., Yao, Y., Hao, H., & Li, L. (2023). Alteration of Excitation/Inhibition Imbalance in the Hippocampus and Amygdala of Drug-Resistant Epilepsy Patients Treated with Acute Vagus Nerve Stimulation. Brain Sciences, 13(7), 976. https://doi.org/10.3390/brainsci13070976

Panuccio, G., Colombi, I., & Chiappalone, M. (2018). Recording and Modulation of Epileptiform Activity in Rodent Brain Slices Coupled to Microelectrode Arrays. Journal of Visualized Experiments, 135. https://doi.org/10.3791/57548

Pfammatter, J. A., Bergstrom, R. A., Wallace, E. P., Maganti, R. K., & Jones, M. V. (2018). A predictive epilepsy index based on probabilistic classification of interictal spike waveforms. PLOS ONE, 13(11), e0207158. https://doi.org/10.1371/journal.pone.0207158

Pinheiro, D. J. L. L., Oliveira, L. F., Souza, I. N. O., Brogin, J. A. F., Bueno, D. D., Miranda, I. A., Da Poian, A. T., Ferreira, S. T., Figueiredo, C. P., Clarke, J. R., Cavalheiro, E. A., & Faber, J. (2020). Modulation in phase and frequency of neural oscillations during epileptiform activity induced by neonatal Zika virus infection in mice. Scientific Reports, 10(1), 6763. https://doi.org/10.1038/s41598-020-63685-2

Pinto, M., Coelho, T., Leal, A., Lopes, F., Dourado, A., Martins, P., & Teixeira, C. (2022). Interpretable EEG seizure prediction using a multiobjective evolutionary

algorithm. Scientific Reports, 12(1), 4420. https://doi.org/10.1038/s41598-022-08322-w

Raimondo, J. V., Heinemann, U., Curtis, M., Goodkin, H. P., Dulla, C. G., Janigro, D., Ikeda, A., Lin, C. K., Jiruska, P., Galanopoulou, A. S., & Bernard, C. (2017). Methodological standards for in vitro models of epilepsy and epileptic seizures. A <scp>TASK</scp> 1- <scp>WG</scp> 4 report of the <scp>AES</scp> / <scp>ILAE</scp> Translational Task Force of the ILAE. Epilepsia, 58(S4), 40–52. https://doi.org/10.1111/epi.13901

Sheybani, L., Mégevand, P., Spinelli, L., Bénar, C. G., Momjian, S., Seeck, M., Quairiaux, C., Kleinschmidt, A., & Vulliémoz, S. (2021). Slow oscillations open susceptible time windows for epileptic discharges. Epilepsia, 62(10), 2357–2371. https://doi.org/10.1111/epi.17020

Sorokin, J. M., Davidson, T. J., Frechette, E., Abramian, A. M., Deisseroth, K., Huguenard, J. R., & Paz, J. T. (2017). Bidirectional Control of Generalized Epilepsy Networks via Rapid Real-Time Switching of Firing Mode. Neuron, 93(1), 194–210. https://doi.org/10.1016/j.neuron.2016.11.026

Sorokin, J. M., Paz, J. T., & Huguenard, J. R. (2016). Absence seizure susceptibility correlates with pre-ictal β oscillations. Journal of Physiology-Paris, 110(4), 372–381. https://doi.org/10.1016/j.jphysparis.2017.05.004

Traynelis, S. F., & Dingledine, R. (1988). Potassium-induced spontaneous electrographic seizures in the rat hippocampal slice. Journal of Neurophysiology, 59(1), 259–276. https://doi.org/10.1152/jn.1988.59.1.259

Traynelis, S. F., Dlugos, D., Henshall, D., Mefford, H. C., Rogawski, M. A., Staley, K. J., Dacks, P. A., Whittemore, V., & Poduri, A. (2020). Epilepsy Benchmarks Area III: Improved Treatment Options for Controlling Seizures and Epilepsy-Related Conditions Without Side Effects. Epilepsy Currents, 20(1_suppl), 23S-30S. https://doi.org/10.1177/1535759719895279

van van Hugte, E. J. H., Schubert, D., & Nadif Kasri, N. (2023). Excitatory/inhibitory balance in epilepsies and neurodevelopmental disorders: Depolarizing γ-aminobutyric acid as a common mechanism. Epilepsia, 64(8), 1975–1990. https://doi.org/10.1111/epi.17651

Vila-Merkle, H., González-Martínez, A., Campos-Jiménez, R., Martínez-Ricós, J., Teruel-Martí, V., Lloret, A., Blasco-Serra, A., & Cervera-Ferri, A. (2023). Sex differences in amygdalohippocampal oscillations and neuronal activation in a rodent anxiety model and in response to infralimbic deep brain stimulation. Frontiers in Behavioral Neuroscience, 17. https://doi.org/10.3389/fnbeh.2023.1122163

Wang, C., Furlong, T. M., Stratton, P. G., Lee, C. C. Y., Xu, L., Merlin, S., Nolan, C., Arabzadeh, E., Marek, R., & Sah, P. (2021). Hippocampus–Prefrontal Coupling Regulates Recognition Memory for Novelty Discrimination. The Journal of Neuroscience, 41(46), 9617–9632. https://doi.org/10.1523/JNEUROSCI.1202-21.2021

Wu, Y.-J., Chien, M.-E., Chiang, C.-C., Huang, Y.-Z., Durand, D. M., & Hsu, K.-S. (2021). Delta oscillation underlies the interictal spike changes after repeated transcranial direct current stimulation in a rat model of chronic seizures. Brain Stimulation, 14(4), 771–779. https://doi.org/10.1016/j.brs.2021.04.025

Xydias, D., Ziakas, G., Psilodimitrakopoulos, S., Lemonis, A., Bagli, E., Fotsis, T., Gravanis, A., Tzeranis, D. S., & Stratakis, E. (2021). Three-dimensional characterization of collagen remodeling in cell-seeded collagen scaffolds via polarization second harmonic generation. Biomedical Optics Express, 12(2), 1136. https://doi.org/10.1364/BOE.411501

Yaari, Y., Konnerth, A., & Heinemann, U. (1986). Nonsynaptic epileptogenesis in the mammalian hippocampus in vitro. II. Role of extracellular potassium. Journal of Neurophysiology, 56(2), 424–438. https://doi.org/10.1152/jn.1986.56.2.424

Yan, J., Li, J., Xu, H., Yu, Y., & Xu, T. (2022). Seizure Prediction Based on Transformer Using Scalp Electroencephalogram. Applied Sciences, 12(9), 4158. https://doi.org/10.3390/app12094158

Yang, Y., Zhou, M., Niu, Y., Li, C., Cao, R., Wang, B., Yan, P., Ma, Y., & Xiang, J. (2018). Epileptic Seizure Prediction Based on Permutation Entropy. Frontiers in Computational Neuroscience, 12. https://doi.org/10.3389/fncom.2018.00055